Structure and Predictability of the El Niño/Southern Oscillation Phenomenon in a Coupled Ocean–Atmosphere General Circulation Model

M. LATIF, A. STERL,* E. MAIER-REIMER, AND M. M. JUNGE

Max-Planck-Institut für Meteorologie, Hamburg, Germany

(Manuscript received 6 February 1992, in final form 20 July 1992)

ABSTRACT

The space–time structure and predictability of the El Niño/Southern Oscillation (ENSO) phenomenon was investigated. Two comprehensive datasets were analyzed by means of an advanced statistical method, one based on observational data and the other on data derived from an extended-range integration performed with a coupled ocean–atmosphere general circulation model. It is shown that a considerable portion of the ENSO-related low-frequency climate variability in both datasets is associated with a cycle involving slow propagation in the equatorial oceanic heat content and the surface wind field. The existence of this cycle implies the possibility of climate predictions in the tropics up to lead times of about one year. This is shown by conducting an ensemble of predictions with our coupled general circulation model. For the first time a coupled model of this type was successfully applied to ENSO predictions.

1. Introduction

Large-scale air–sea interactions contribute considerably to climate variability on a wide range of time scales. On the short-range climatic time scale up to a few years the El Niño/Southern Oscillation (ENSO) phenomenon is the most prominent representative of such air–sea interactions. Bjerknes (1969) was among the first to describe ENSO as a coupled phenomenon by pointing out the close connection between the atmospheric phenomenon Southern Oscillation and the oceanic phenomenon El Niño, both of which had been known for several decades. El Niño is characterized by the occurrence of anomalously warm surface waters in the entire tropical Pacific for about a year (Rasmusson and Carpenter 1982), while the Southern Oscillation consists basically of a seesaw in surface pressure that involves opposite changes in the eastern and western hemispheres (Berlage 1957). The ENSO phenomenon has received widespread attention, because it not only influences regional and global climate (Rasmusson and Carpenter 1982; Cane 1983; Glantz et al. 1991), but also the ecosystems in the Indo-Pacific region and the economies of several countries (Oceanus 1984).

As shown in Fig. 1a, typical indices of the Southern Oscillation and El Niño [as expressed by the so-called Southern Oscillation index (SOI) and by an index of eastern-equatorial sea surface temperature (SST)] vary coherently out of phase on interannual time scales. As already hypothesized by Bjerknes (1969) these interannual variations arise from an instability of the coupled ocean-atmosphere system in the tropics (e.g., Hirst 1990; Philander 1990). Bjerknes (1969) introduced the concept of the Walker circulation (named after the discoverer of the Southern Oscillation, Sir Gilbert Walker), a thermodynamically direct atmospheric circulation cell parallel to the equator. The driving force for the Walker circulation is the zonally asymmetric distribution of convection caused by the characteristic zonal SST gradient across the equatorial Pacific. A negative anomaly in the SOI, for instance, corresponds to a weak pressure gradient across the Pacific, resulting in weak trade winds. Since the SST in the eastern Pacific evolves as a dynamic response to the surface wind field, a drop in the SOI leads to warmer conditions in the eastern Pacific and to a weaker zonal SST gradient due to reduced upwelling of cold waters from below. The reduction in the east–west temperature contrast reduces the strength of the Walker circulation so that the zonal winds along the equator are further weakened, which further weakens the zonal SST gradient and so on. Conversely, a positive anomaly in the SOI is accompanied by stronger winds and upwelling, resulting in colder than normal SSTs and an increased zonal SST gradient, which leads to an intensified Walker circulation and stronger winds which further lower the SSTs in the eastern Pacific. Hence, any initial disturbance tends to be amplified by unstable air–sea interactions.

ENSO can be described as an oscillation between a

* Current affiliation: KNMI, de Bilt, the Netherlands.

Corresponding author address: M. Latif, Max-Planck-Institut für Meteorologie, Bundesstrasse 55, 2000 Hamburg 13, Germany.

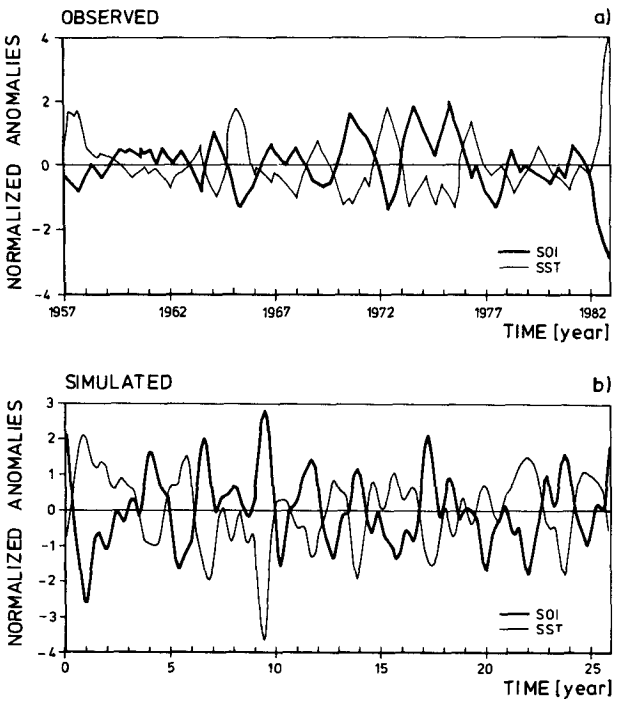

FIG. 1. (a) Time series of the Southern Oscillation index as defined by the anomalous pressure difference between Tahiti (French Polynesia) and Darwin (Australia) and of anomalous SST in the eastern Pacific (Puerto Chicama, Peru) (redrawn after Oceanus 1984). (b) Same as in (a) but derived from the extended-range integration with the coupled ocean–atmosphere GCM (Latif et al. 1992). The model SOI is defined as the anomalous pressure difference between an average over the eastern Pacific and the Indian Ocean. SST anomalies have been averaged over the Niño-3 region, which is an average over the eastern equatorial Pacific. All time series are normalized by their long-term standard deviation.

warm and a cold phase, which are commonly referred to as El Niño and La Niña, respectively (Barnett 1985; Wyrtki 1985; Zebiak and Cane 1987; Van Loon and Shea 1987; Schopf and Suarez 1988; Graham and White 1988; Battisti and Hirst 1989; Philander 1990; Xu and Storch 1990; Cane et al. 1990; Münnich et al. 1991; Philander et al. 1992); however, although there is a wide consensus of how anomalies grow during the extremes of ENSO, a number of competing hypotheses have been proposed for the maintenance of the ENSO cycle. Here, we further investigate the ENSO mechanism by analyzing observational data from different sources and by analyzing the results of a coupled ocean–atmosphere general circulation model. We use an advanced statistical method based on the principal oscillation pattern (POP) technique to derive the characteristic space–time structure from the data. We also discuss the issue of ENSO predictability. It is shown by running our coupled ocean-atmosphere general circulation model in the predictive mode that ENSO predictions are possible up to lead times of at least one year.

2. Data

a. Observations

We used in our analysis bimonthly anomalies of SST (Graham and White 1990), zonal surface wind stress (Goldenberg and O'Brien 1981; Legler and O'Brien 1984) and the depth of the 20°C isotherm (K. Mizuno and W. White, personal communication) (a measure of upper-ocean heat content) in the region 10°N to 10°S. It is known from linear stability analysis that these three quantities are the most important ones in tropical air–sea interactions. The analyzed period extends from 1967 to 1986. Sea surface temperatures and wind-stress anomalies cover the domain 124°E to 80°W. The 20°C isotherm data were only available for the domain 120°E to 140°W. The data coverage for this dataset, especially in the first half of the analyzed period, is poor, resulting in large spatial and temporal gaps. These gaps have been simply filled with climatology or equivalently with zero anomaly. Nevertheless, observations with such a spatial and temporal coverage have not been used before in a simultaneous statistical analysis. To remove high-frequency noise and fluctuations with periods much longer than the characteristic ENSO period of a few years, we bandpass-filtered the data retaining variations on time scales of 16–120 months. Each of the three quantities was then normalized with its spatially averaged standard deviation so that all have the same weight in the statistical analysis.

b. Model data

In addition, we used data derived from a 26-year integration with a coupled ocean–atmosphere general circulation model (Latif et al. 1993), which is based on a high-resolution tropical ocean model and a global low-order spectral atmosphere model. The two models have been coupled without applying any correction to the fluxes (Sausen et al. 1988). The coupled model simulates realistically the interannual variability, as can be inferred from the anomaly time series of the Southern Oscillation index and eastern equatorial SST (Fig. 1b). As in the observations (Fig. 1a), both indices vary coherently out of phase and fluctuate irregularly on time scales of a few years.

We used monthly anomalies of SST, zonal wind stress, and sea level in the region 10°N to 10°S. Sea level was chosen instead of the 20°C isotherm, because it is also a good measure of upper-ocean heat content and readily available from the model output. To reduce spinup problems, we omitted the first two years of the integration. Zonally we use the anomalies between 140°E and 90°W. Prior to the statistical analysis the data were low-pass filtered, retaining variations on time scales longer than a year, and the three model quantities were normalized with their spatially averaged standard deviation.

3. Statistical description of ENSO

a. Statistical method

Our statistical investigation of the space–time structure of ENSO is based on the method of principal oscillation patterns (POPs), which is designed to extract the dominant modes of variability from a multidimensional dataset (Hasselmann 1988; Storch et al. 1988; Xu and Storch 1990). The POPs are the eigenvectors of the system matrix obtained by fitting the data to a multivariate first-order Markov process. POPs are in general complex with real part p_1 and imaginary part p_2. The corresponding complex coefficient time series satisfy the standard damped harmonic oscillator equation, so that the evolution of the system in the two-dimensional POP space can be interpreted as a cyclic sequence of spatial patterns

$$\cdots \rightarrow p_1 \rightarrow -p_2 \rightarrow -p_1 \rightarrow p_2 \rightarrow p_1 \rightarrow \cdots \quad (1)$$

The characteristic period to complete a full cycle will be referred to as rotation period and the e-folding time for exponential decay as damping time. The two time scales are estimated as part of the POP analysis. In our case, in which we consider simultaneously both atmospheric and oceanic quantities, the POPs can be regarded as the eigenmodes of the coupled ocean–atmosphere system.

b. Results

We consider only the most energetic POP mode derived from each of the two datasets. These POP modes are clearly associated, in both the observations and the coupled model, with the ENSO cycle, as was inferred from the corresponding POP coefficient time series (not shown). In both datasets the next energetic POP mode is associated with a biennual rotation period. All other POP modes either are associated with rotation periods significantly different from the ENSO time scale or are statistically not significant. In the following, the real part p_1 of a leading POP mode shows conditions during the warm extreme (El Niño), while the imaginary part p_2 shows the conditions during the transition phase of the ENSO cycle, a quarter of the rotation period previously (precursor patterns). The evolution of the cold extreme of the ENSO cycle (La Niña) is given within this linear concept by the same patterns, but with reversed signs.

The leading POP mode derived from the observations (Fig. 2), which explains about 24% of the total variance, has a rotation time of 39 months and a damping time of 48 months. The corresponding POP coefficient time series (not shown) are dominated by the major warm events of 1972 and 1982–1983 and the two cold episodes after these two warm phases.

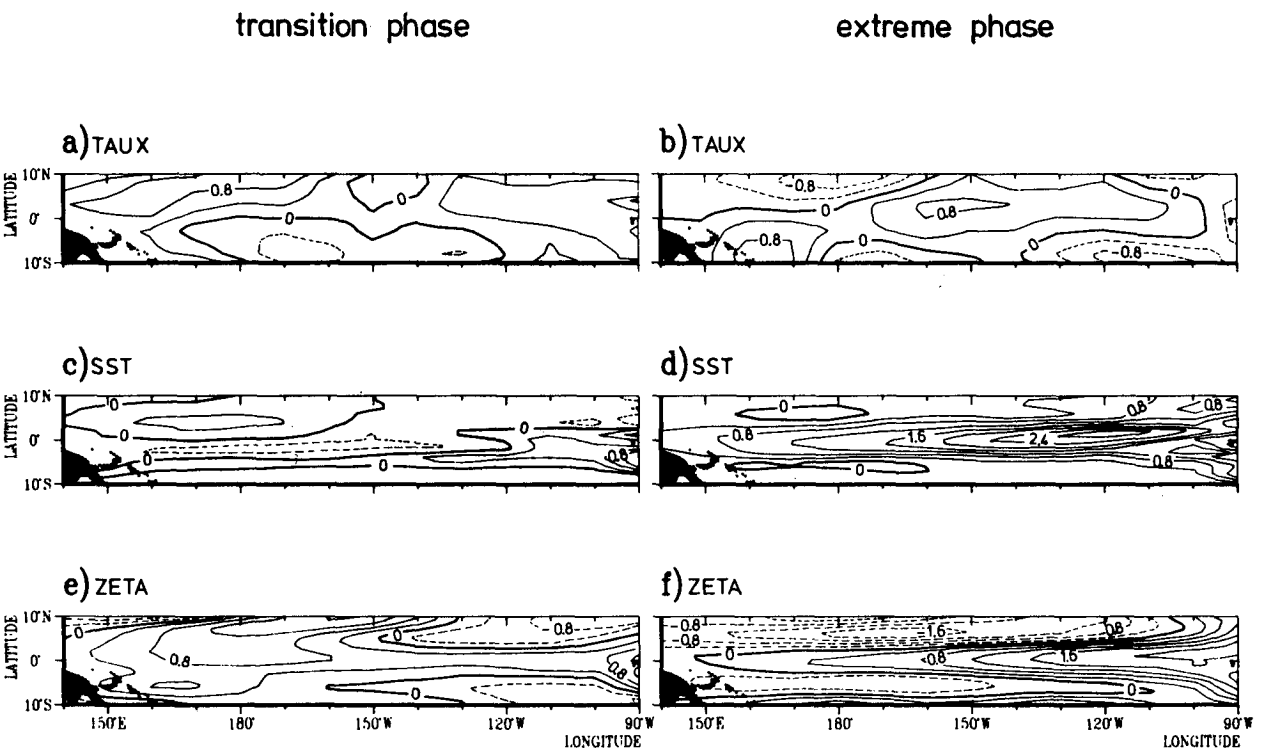

FIG. 2. Evolution of anomalies as derived from the first POP mode of the observations. The panels on the lhs show the transition phase patterns of (a) zonal wind stress, (c) SST, and (e) of the depth of the 20°C isotherm, which precede the warm extreme by about ten months. The panels on the rhs show (b) the anomalous zonal wind stress, (d) SST, and (f) depth of the 20°C isotherm during the warm extreme.

During the extreme phase, the variability patterns show the well known features (Figs. 2b,d,f). There is a large-scale warming centered in the eastern equatorial Pacific (Fig. 2d). This warming is accompanied by westerly wind anomalies displaced to the west of the SST anomalies and centered at the equator near the dateline (Fig. 2b). Heat content anomalies (Fig. 2f), as expressed by the anomalies of the 20°C isotherm, are negative in the western Pacific with the strongest signals off the equator, and there is an indication of positive heat content anomalies at the equator in the central Pacific. This is consistent with a zonal redistribution of heat, as described by many authors (e.g., Wyrtki 1985).

A quarter of the rotation period ten months prior to the warm extreme, ocean and atmosphere seem to be decoupled over the tropical Pacific. Sea surface temperature anomalies (Fig. 2c) are in general weak, so that the evolution of SST can be described to first order as a standing oscillation. The SST field appears to be dominated by a large-scale north–south asymmetry with weak positive anomalies north of and at the equator and weak negative anomalies south of the equator. Although SST anomalies are weak, meridional SST gradients are not negligible in the central equatorial Pacific. It should be noted that SST anomalies occasionally show either westward or eastward propagation (Rasmusson and Carpenter 1982; Gill and Rasmusson 1983). The different propagation characteristics, however, may be averaged out by our POP analysis.

Strong signals can be identified in the precursor pattern of zonal wind stress (Fig. 2a) and upper-ocean heat-content anomalies (Fig. 2e). The precursor pattern of the 20°C isotherm shows a signal in equatorial heat content that is centered at the equator (Fig. 2e). These heat-content anomalies were presumably generated during the preceding cold phase (Fig. 2f with reversed signs) and then "reflected" at the western boundary. Overall the evolution of equatorial heat content is consistent with equatorial wave dynamics summarized in a conceptional model, the delayed action oscillator (Schopf and Suarez 1988), in its generalized form (Philander 1990). According to the delayed action oscillator the ocean is not in equilibrium with the atmosphere and has a memory of past winds. The simplest version of the delayed action oscillator involves only single-wave modes. According to this picture, the easterly wind anomalies over the western Pacific prevailing during La Niña force an upwelling Kelvin wave, which propagates eastward along the equator and causes cooling in the eastern Pacific, where the thermocline is shallow. The ocean response to the easterly winds in the west, however, consists also of a downwelling Rossby wave, which propagates westward. This Rossby wave has its strongest signals off the equator. It does not influence the SST, because the thermocline is deep in the western Pacific. The Rossby wave then reflects at the western boundary into a downwelling Kelvin wave, which propagates eastward along the equator. Once it gets far enough into the eastern Pacific, it is able to affect the SST and, if the signal is strong enough, a positive SST anomaly develops, which can grow by air–sea interactions into an El Niño.

The interpretation in terms of single-wave modes is, however, problematic (Philander 1990). At low frequencies many wave modes are excited so that the propagation speeds would be expected to be much slower than those expected for single waves (Cane and Sarachik 1981). This is supported by our POP analysis (Fig. 2). The estimated phase speed obtained by following the anomalies in the 20°C isotherm in the POP patterns p_1 and p_2 (Figs. 2e,f) is about 25 cm s^{-1}, which is about an order of magnitude less than the speed of the gravest Kelvin wave mode. It should be noted that estimates of time scales are subject to large uncertainties due to the short record length. The main conclusion, however, that the observed phase propagation is much slower than that of individual Kelvin waves, is not affected by this uncertainty.

The precursor pattern of the zonal wind-stress anomaly shows the occurrence of a large-scale westerly anomaly north of the equator, centered in the western Pacific near 150°E (Fig. 2a). Thus the zonal wind stress also involves a propagating mode. Most studies have attributed this feature to an interaction of the Pacific trade wind field with processes outside the tropical Pacific (Barnett 1983; Van Loon and Shea 1987). Other studies relate the propagation in the zonal wind to an internal low-frequency mode in the atmosphere; however, it is also possible that the wind anomaly is directly forced by the meridional SST gradient in the central Pacific (Fig. 2c), because the surface waters are very warm in this region, so that even small changes in SST can have a significant impact on the atmospheric circulation.

The leading POP mode derived from the extended range integration with the coupled general circulation model (Fig. 3) explains 28% of the variance and is associated with a rotation period of 32 months and a damping time of 27 months. The relatively short damping time might indicate that the coupled model is less unstable than the real world; however, as just stated, estimates of time scales from such relatively short records are subject to large uncertainties. Overall, the ENSO evolution in the coupled model (Fig. 3) appears to be very similar to the observed evolution (Fig. 2). While zonal wind-stress and heat-content anomalies are dominated by a propagating mode, SST anomalies evolve approximately as a standing oscillation.

The warm extreme is characterized by large-scale warming centered in the eastern-equatorial Pacific (Fig. 3d). The meridional extent of the SST anomalies, however, is considerably underestimated by the cou-

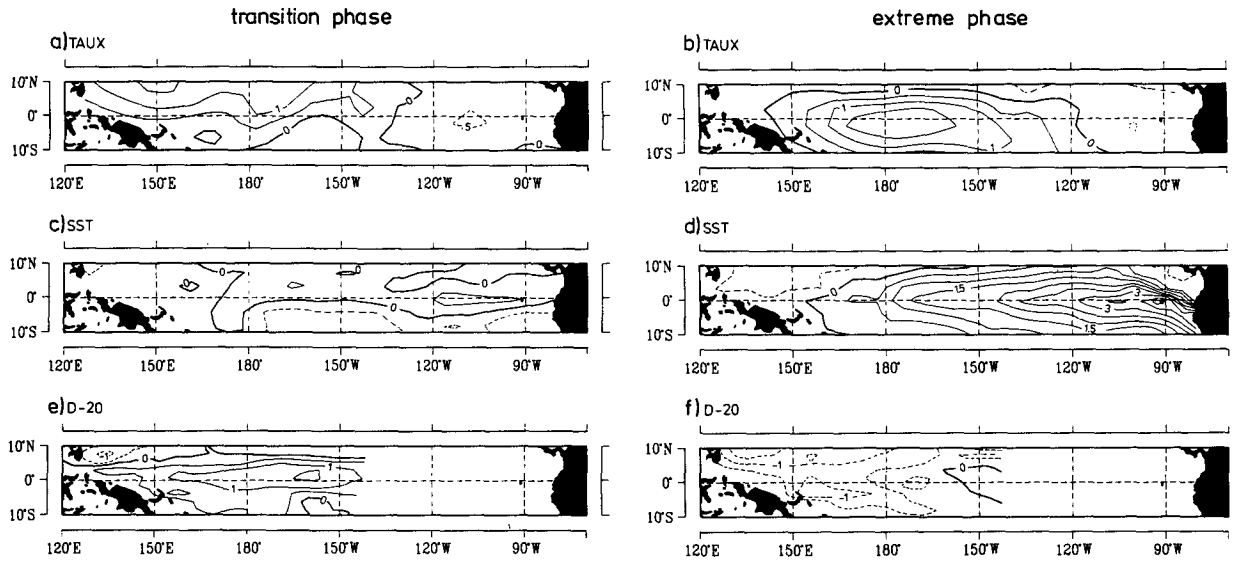

FIG. 3. As Fig. 2, but as derived from the run with the coupled ocean–atmosphere GCM. Instead of the depth of the 20°C isotherm, sea level was used as a measure of upper-ocean heat content in (e) and (f).

pled model. The warming is accompanied by westerly wind anomalies (Fig. 3b). Although the occurrence of westerly wind anomalies is consistent with the observations (Fig. 2b), they are not simulated far enough west of the SST anomalies, being centered near 150°W. The sea level during the El Niño phase shows an increase in heat content in the eastern and a reduction in heat content in the western Pacific. Positive anomalies in the east are centered at the equator and exhibit a Gaussian shape. The negative heat content anomalies in the west are strongest off the equator at about 7°N and 7°S. Such a structure in heat content is reminiscent of Rossby and Kelvin wave structure.

The gross features of the precursor patterns (Figs. 3a,c,e) are also consistent with the observations (Figs. 2a,c,e). SST anomalies are rather weak and dominated by a north–south asymmetry with a moderate meridional gradient near the equator in the central Pacific (Fig. 3c); however, compared with the observations (Fig. 2c), the position of the region of strongest meridional gradient is somewhat displaced to the west. Nevertheless, it is interesting that the evolution of SST in the coupled model also involves a transition from a meridionally asymmetric state (Fig. 3c) to a zonally asymmetric state (Fig. 3d). The precursor pattern of the sea level anomalies indicates that in the coupled model equatorial wave activity is also important (Fig. 3e). Positive heat-content anomalies, generated during the negative extreme (Fig. 3f, but with reversed signs), propagate slowly eastward along the equator. The estimated phase speed by which anomalies propagate along the equator is about 20 cm s^{-1}. As in the observations, this is much slower than the gravest Kelvin wave speed.

The coupled model also simulates the observed occurrence of westerly wind-stress anomalies in the northwestern Pacific (Fig. 3a) so that the model stress is also characterized by a slowly eastward propagating mode. Since the westerly wind patch over the northwest is clearly related to the meridional temperature gradient in this region (Fig. 3c), the results of the coupled model support the hypothesis that the observed slow eastward propagation in zonal wind prior to El Niño is caused by coupled processes within the tropical Pacific region itself; however, more measurements and model studies are needed to address this point adequately.

4. ENSO predictability

The POP analyses of both the observations and the results of the coupled model integration show clearly that a large portion of the ENSO-related low-frequency variability can be described as a cycle within the coupled ocean–atmosphere system. Since the evolution of the ENSO cycle appears to be similar in two independent datasets, one based on observations and the other on the results of a coupled model, we have some confidence in the derived variability patterns. To further investigate the reliability of our results, we conducted ENSO predictions by means of a statistical prediction scheme and with our coupled general circulation model.

The applied POP technique contains an inherent, rather simple prediction scheme (Xu and Storch 1990) that works as follows. First, the coupled ocean–atmo-

sphere system is projected into the two-dimensional POP space. The prediction then simply consists of a damped rotation within the POP space, because the POP coefficients fulfill the standard damped harmonic oscillator equation. If, for instance, the coupled system is in a state that corresponds to the transition phase patterns given in Fig. 2, then a quarter of the rotation period later, the coupled system is assumed to be in the warm extreme phase. After the rotation in the POP space the fields are reconstructed and verifications of the predictions can be made.

We initialized predictions for each bimonth during the period 1967 to 1986. This yields 120 predictions in total. Each prediction has a duration of one 16 months. Verifications are made for central equatorial SST anomalies averaged over the so-called SST-3 region, which is an area average over the region 5°N–5°S and 170°W–120°W (Fig. 4, upper). The results of the predictions are summarized in the lower panel of Fig. 4, which shows the anomaly correlation coefficient between the predicted and the (unfiltered) observed SST anomalies as a function of the forecast lag. The anomaly correlations were computed by subtracting the sample means. Also shown are the results of the persistence forecast, which assumes that the initial SST anomaly is constant throughout the forecast period. Central equatorial Pacific SST anomalies are predictable about one year in advance with our simple statistical prediction scheme (a correlation of 0.5 is commonly regarded as a threshold value for useable predictions). This result provides further support that our statistical description of the ENSO cycle captures important aspects of the true ENSO cycle.

Our skills are considerably higher than those obtained by using atmospheric data only in statistical ENSO predictions (Xu and Storch 1990; Graham et al. 1987). Further, the skills decrease considerably if only the observed wind stresses were used in a POP prediction scheme (not shown), while they remain basically unchanged when only the 20°C-isotherm data were used. These results indicate the importance of subsurface processes for the maintenance of the ENSO cycle. Similar results were obtained by Latif and Graham (1992). They showed that by forcing an ocean model with the observed wind stresses and using the model's subsurface temperatures instead of the stresses themselves as predictors remarkably increases the skill in predicting the observed SST changes.

The results of the statistical predictions (Fig. 4) should be taken with some caution, because the POP model was derived from the same time period for which predictions were made. Furthermore, bandpass filtering was applied to the data, which also introduces some "artificial" skill. As pointed out by Xu and Storch (1990), however, the artificial skill of the POP prediction scheme is expected to be small, because only a single dominant POP mode was used in the predictions.

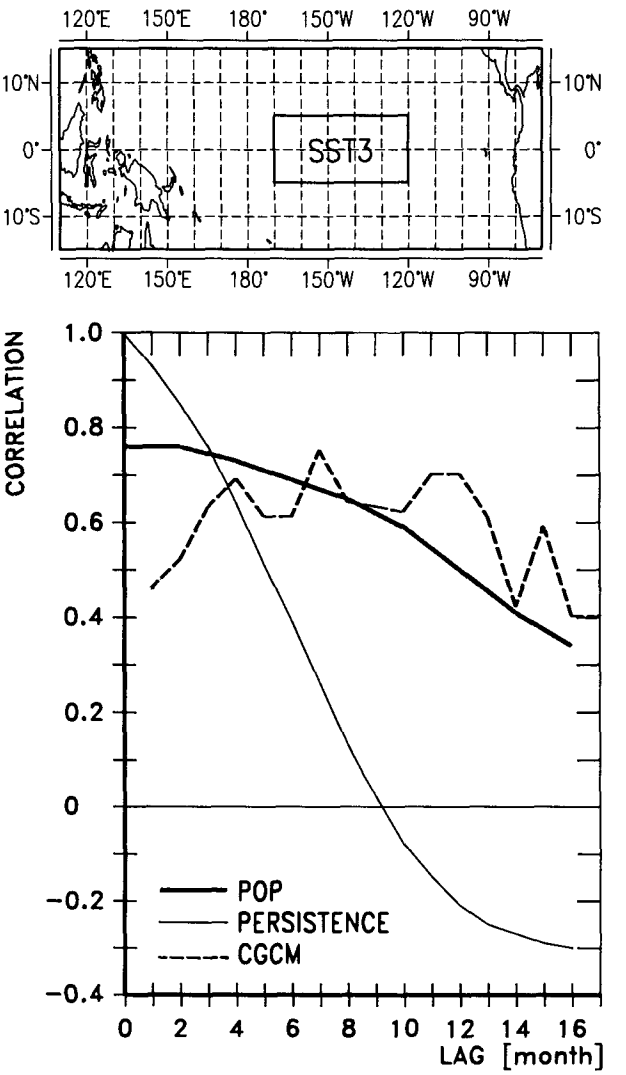

FIG. 4. Upper: SST-3 region used for averaging and verifying the results of the ENSO predictions. Lower: Anomaly correlation coefficients of the ENSO predictions with the CGCM as a function of the forecast lag. The dashed curve shows the correlations obtained if the predictions are verified with respect to the observed SST anomalies. The thick curve labeled POP shows the hindcast correlations obtained from the POP model. For comparison the results of the persistence forecast are shown by the thin line.

Nevertheless, the results of the statistical predictions should be regarded as "hindcasts" and therefore as an upper limit for the predictability with our POP prediction scheme.

We then applied our coupled general circulation model to the prediction of tropical Pacific SST. As in numerical weather prediction, ENSO prediction poses an initial value problem (Cane et al. 1986; Goswami and Shukla 1991). Oceanic initial conditions for the predictions were taken from an uncoupled run, in which the ocean model was forced by observed wind-

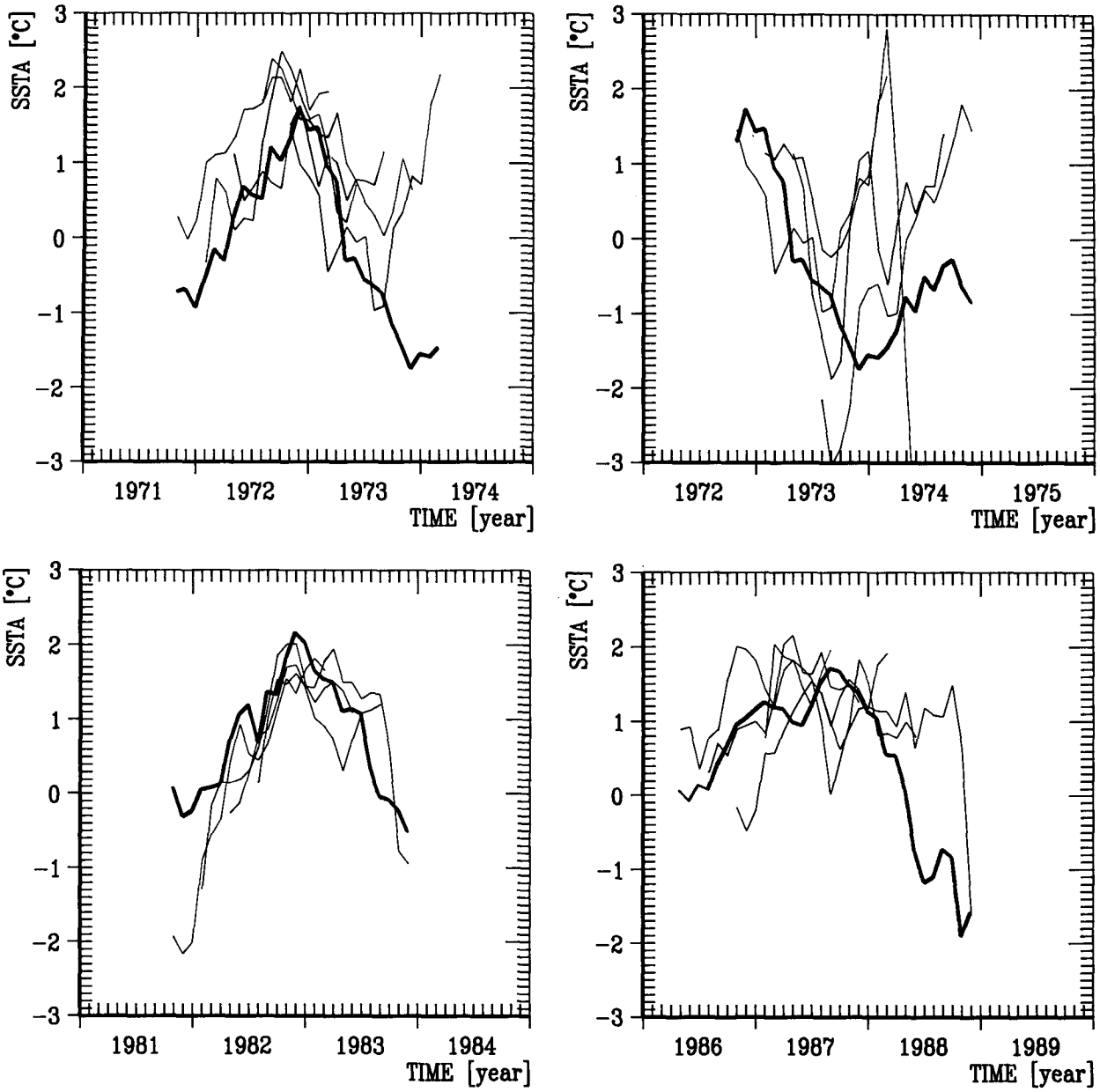

FIG. 5. Individual forecasts with the coupled GCM. The thick lines shows the observed changes in SST-3 temperature anomalies, while the dashed lines show the twenty individual coupled GCM forecasts. The initialization dates of the forecasts are: Sep 1971, Dec 1971, Mar 1972, Jun 1972, Sep 1972, Dec 1972, Mar 1973, Jun 1973, Sep 1981, Dec 1981, Mar 1982, Jun 1982, Mar 1986, Jun 1986, Sep 1986, Dec 1986, Jun 1987, Sep 1987, Dec 1987, Mar 1988.

stress anomalies taken from the Florida State University dataset (Goldenberg and O'Brien 1981; Legler and O'Brien 1984) which were added to the wind-stress climatology derived from the 26-year coupled control integration. We used the raw wind-stress anomalies to spin up the ocean model, that is, no filtering or detrending was applied, so that no future information was used in the prediction experiments. Atmospheric initial conditions were obtained by forcing the atmospheric GCM for one month by the SSTs simulated by the ocean GCM in the uncoupled run just described. This initialization procedure minimizes the climate drift problem. Since the coupled GCM (CGCM) was run in a real forecast mode, its skill can be referred to as forecast skill. For each case four different initial conditions three months apart from each other were used.

Due to restrictions in computer facilities, we performed an ensemble of only 20 predictions. Predictions were made for the El Niños 1972, 1982–1983, and 1986–1987 and for the La Niñas of 1973 and 1988

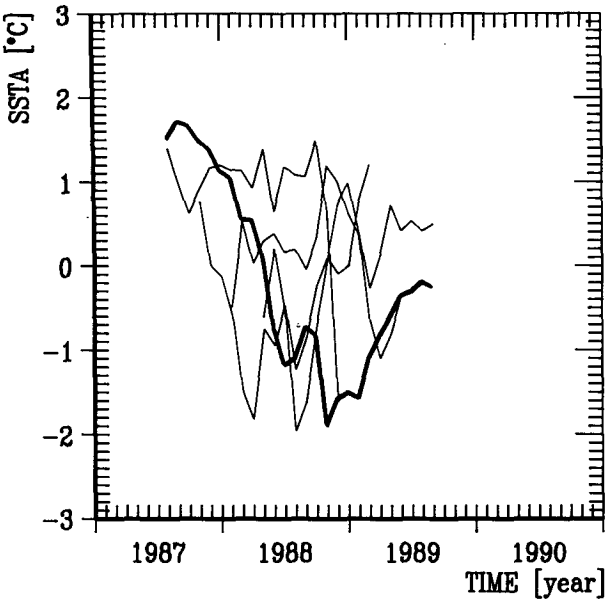

FIG. 5. (*Continued*)

(Fig. 5). Model-SST anomalies are computed by subtracting from the forecasts the coupled model's SST climatology derived from the 26-year coupled control integration. The results of the predictions are then compared to the (unfiltered) observed SST anomalies in the SST-3 region, which were obtained by removing the annual cycle from the SST data. The coupled model is successful in predicting the observed changes in SST. Substantial correlations are found for forecast lags beyond one year (Fig. 4, lower); however, the skill of our CGCM may be exaggerated by the fact that we chose only "active" periods for our prediction experiments. Thus, comparisons with the overall POP results shown in the same figure are premature. Consequently, results for the 16 cases common to both the CGCM and POP experiments are shown in Fig. 6. Keep in mind, however, that 1) sampling error can be large for such a small sample and 2) the POP skill may be inflated artificially. Furthermore, it should be mentioned that the shown correlation skill represents an average value over all seasons. Other studies have shown that the skills critically depend on the season with SST anomalies in spring being least predictable (e.g., Latif and Graham 1992); however, our ensemble of predictions is too small to estimate the seasonal dependence of our CGCM's skill, but we made sure that the initialization dates were distributed homogeneously with respect to the annual cycle.

5. Conclusions

We have investigated the space–time structure of the ENSO phenomenon by means of a statistical analysis and discussed the issue of ENSO predictions. By using both observational data and data from a coupled ocean-atmosphere general circulation model in our statistical description of ENSO the results provide not only insight into the nature of ENSO but also a basis for comparison of the performance of our coupled model with observations. Our results show that ENSO is definitely based on a cycle that involves standing SST anomalies and slow propagation in the upper-ocean heat content and the surface wind field. Variations in the oceanic heat content are clearly associated with the propagation of equatorial waves as expressed by the delayed action oscillator (Schopf and Suarez 1988; Graham and White 1988) in its generalized form (Philander 1990).

The applied statistical technique of principal oscillation patterns is a convenient and powerful method to verify climate models. By comparing the dominant POP modes derived from the observations and the coupled model we have shown that present state of the art coupled general circulation models are successful in simulating important aspects of the observed interannual variability in the tropical Pacific. As in the observations, the model ENSO exhibits a strong cyclic component and similar propagation characteristics in all three analyzed quantities.

The existence of a cycle enables ENSO predictions to be made up to lead times of about one year, and

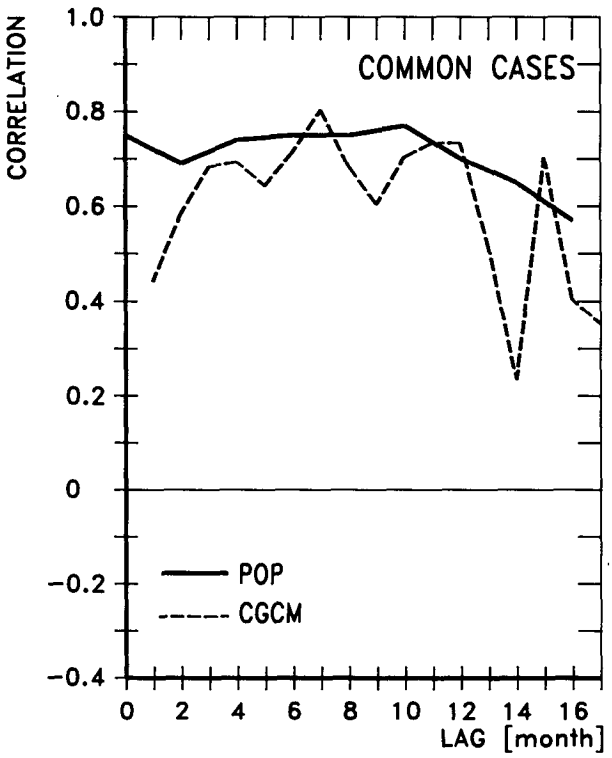

FIG. 6. Anomaly correlation coefficients of the ENSO predictions with the coupled GCM and the POP model, when both models are applied to the 16 common cases.

this has been confirmed by our statistical predictions and predictions with our coupled ocean–atmosphere general circulation model. One major result from this study is certainly that skillful ENSO predictions are possible with coupled ocean–atmosphere general circulation models, despite the fact that these models still suffer from serious climate drift (Neelin et al. 1992; Latif et al. 1993). Further, since important quantities for tropical large-scale air–sea interactions, such as SST, heat content, and zonal wind can be measured with some accuracy from space, we can expect further progress in ENSO predictions by assimilating satellite data into coupled ocean–atmosphere general circulation models.

Acknowledgments. We enjoyed discussions with Drs. Tim Barnett, Mark Cane, David Neelin, and George Philander. We would like to thank Dr. R. Livezey for his critical comments on an earlier version of the manuscript. We thank Prof. J. J. O'Brien for providing the wind-stress data, Dr. N. E. Graham for providing the SST data, and Drs. W. B. White and K. Mizuno for the 20°C-isotherm data. Many thanks to Mrs. Marion Grunert and to Mr. N. Noreiks for preparing the diagrams. Part of the work was sponsored by the Tropical Ocean Global Atmosphere (TOGA) Programme, by the European Community Climate Program under Grant EV4C-0035-D(B), and by the Körber Projekt. The coupled integrations have been carried out at the Deutsches Klimarechenzentrum.

REFERENCES

Barnett, T. P., 1983: Interaction of the Monsoon and the Pacific trade wind system at interannual time scales. Part I: The equatorial zone. *Mon. Wea. Rev.*, **111**, 756–773.

——, 1985: Variations in near global sea level pressure. *J. Atmos. Sci.*, **42**, 478–501.

Battisti, D. S., and A. C. Hirst, 1989: Interannual variability in a tropical atmosphere-ocean model: Influence of the basic state, ocean geometry and nonlinearity. *J. Atmos. Sci.*, **46**, 1687–1712.

Berlage, H. P., 1957: Fluctuations in the general atmospheric circulation of more than one year, their nature and prognostic value. K. Ned. Meteor. Inst. Meded. Verh., 69.

Bjerknes, J., 1969: Atmospheric teleconnections from the equatorial Pacific. *Mon. Wea. Rev.*, **97**, 163–172.

Cane, M. A., 1983: Oceanographic events during El Niño. *Science*, **222**, 1189–1195.

——, and E. S. Sarachik, 1981: The response of a linear baroclinic equatorial ocean to periodic forcing. *J. Mar. Res.*, **39**, 651–693.

——, S. E. Zebiak, and S. C. Dolan, 1986: Experimental forecasts of El Niño. *Nature*, **321**, 827–832.

——, M. Münnich, and S. E. Zebiak, 1990: A study of self-excited oscillations of the tropical ocean-atmosphere system. Part I: Linear analyses. *J. Atmos. Sci.*, **47**, 1562–1577.

Gill, A. E., and E. M. Rasmusson, 1983: The 1982–83 climate anomaly in the equatorial Pacific. *Nature*, **306**, 229–234.

Glantz, M. H., 1984: Floods, bias, famine. Is El Niño to blame? *Special Issue: El Niño, Oceanus*, **27**, 14–18.

——, R. W. Katz, and N. Nicholls, 1991: *Teleconnections Linking Worldwide Climate Anomalies.* Cambridge University Press, 535 pp.

Goldenberg, S. O., and J. J. O'Brien, 1981: Time and space variability of tropical Pacific wind stress. *Mon. Wea. Rev.*, **109**, 1190–1207.

Goswami, B. N., and J. Shukla, 1991: Predictability of a coupled ocean–atmosphere model. *J. Climate*, **4**, 3–22.

Graham, N. E., and W. B. White, 1988: The El Niño cycle: A natural oscillator of the Pacific Ocean. *Science*, **240**, 1293–1302.

——, and ——, 1990: The role of the western boundary in the ENSO cycle: Experiments with coupled models. *J. Phys. Oceanogr.*, **20**, 1935–1948.

——, J. Michaelsen, and T. P. Barnett, 1987: An investigation of the El Niño–Southern Oscillation cycle with statistical models. Part II: Model results. *J. Geophys. Res.*, **92**, 14 271–14 289.

Hasselmann, K., 1988: PIPs and POPs: The reduction of complex dynamical systems using principal interaction and oscillation patterns. *J. Geophys. Res.*, **93**, 11 015–11 021.

Hirst, A. C., 1990: On simple coupled ocean-atmosphere models, equatorial instabilities and ENSO. *Proc. Int. TOGA Scientific Conf.*, Honolulu, World Climate Research Programme, WCRP-43, WMO/TD-No. 379, 103–110.

Latif, M., and N. E. Graham, 1992: How much predictive skill is contained in the thermal structure of an OGCM. *J. Phys. Oceanogr.*, **22**, 951–962.

——, A. Sterl, E. Maier-Reimer, and M. M. Junge, 1993: Climate variability in a coupled GCM. Part I: The tropical Pacific. *J. Climate*, **6**, 5–21.

Legler, D. M., and J. J. O'Brien, 1984: *Atlas of Tropical Pacific Wind Stress Climatology 1971–1980.* Florida State University, Dept. of Meteor.

Münnich, M., M. A. Cane, and S. E. Zebiak, 1991: A study of self-excited oscillations of the tropical ocean–atmosphere system. Part II: Nonlinear Cases. *J. Atmos. Sci.*, **48**, 1238–1248.

Neelin, J. D., M. Latif, M. A. F. Allaart, M. A. Cane, U. Cubasch, W. L. Gates, P. R. Gent, M. Ghil, C. Gordon, N. C. Lau, C. R. Mechoso, G. A. Meehl, J. M. Oberhuber, S. G. H. Philander, P. S. Schopf, K. R. Sperber, A. Sterl, T. Tokioka, J. Tribbia, and S. E. Zebiak, 1992: Tropical air–sea interaction in general circulation models. *Climate Dyn.*, **7**, 73–104.

Philander, S. G. H., 1990: A review of simulations of the Southern Oscillation. Proc. Int. TOGA Scientific Conf., Honolulu, World Climate Research Programme, WCRP-43, WMO/TD-No. 379, 87–94.

——, R. C. Pacanowski, N.-C. Lau, and M. J. Nath, 1992: Simulation of ENSO with a global atmospheric GCM coupled to a high-resolution tropical Pacific Ocean model. *J. Climate*, **5**, 308–329.

Rasmusson, E. N., and T. H. Carpenter, 1982: Variations in tropical sea surface temperature and surface wind fields associated with the Southern Oscillation/El Niño. *Mon. Wea. Rev.*, **110**, 354–384.

Sausen, R., K. Barthel, and K. Hasselmann, 1988: Coupled ocean-atmosphere models with flux correction. *Climate Dyn.*, **2**, 145–163.

Schopf, P. S., and M. J. Suarez, 1988: Vacillations in a coupled ocean–atmosphere model. *J. Atmos. Sci.*, **45**, 549–566.

Storch, H. v., T. Bruns, I. Fischer-Bruns, and K. Hasselmann, 1988: Principal Oscillation analysis of the 30 to 60 day oscillation in a GCM. *J. Geophys. Res.*, **93**, 11 022–11 036.

Van Loon, H., and D. J. Shea, 1987: The Southern Oscillation. Part VI: Anomalies of sea level pressure on the Southern Hemisphere and of Pacific sea surface temperature during the development of a warm event. *Mon. Wea. Rev.*, **113**, 370–379.

Wyrtki, K., 1985: Water displacements in the Pacific and the genesis of El Niño cycles. *J. Geophys. Res.*, **90**, 10 419–10 424.

Xu, J.-S., and H. v. Storch, 1990: Principal oscillation patterns—Prediction of the state of ENSO. *J. Climate*, **3**, 1316–1329.

Zebiak, S. E., and M. A. Cane, 1987: A model El Niño–Southern Oscillation. *Mon. Wea. Rev.*, **115**, 2262–2278.